Pergamon

Continental Shelf Research, Vol. 14, No. 13/14, pp. 1455–1475, 1994

0278–4343/94 $7.00 + 0.00

# Oscillatory boundary layer flows modelled with dynamic Reynolds stress turbulence closure

BÅRD BRØRS* and KARL J. EIDSVIK†

(Received 9 July 1992; in revised form 11 May 1993; accepted 27 August 1993)

**Abstract**—A standard dynamic Reynolds stress model, with conventional coefficients, is applied to oscillatory boundary layer flows. With a grid resolution over the boundary layer thickness and wave period of the order of 100 and 600 respectively, well defined, grid-independent solutions are obtained. The available data are predicted in great detail. However, even with turbulence characteristics, the data from oscillatory flows do not appear to be very model discriminant. A model based upon a standard ($k$-$\varepsilon$) closure also predicts them reasonably realistically.

With sediment entrainment, giving stably stratified flow, the Reynolds stress model estimates that there is almost no turbulence above the mean velocity maximum. This is probably a reason why a ($k$-$\varepsilon$) model even predicts such flows accurately. Another reason is that the flow is strongly forced (by the oscillatory pressure gradient) and is not, like for instance turbidity currents, decisively governed by the turbulence.

An oscillatory flow with sediment entrainment on a slope is predicted to force a systematic turbidity current. At large enough slope angles, the waves are predicted to trigger self-accelerated turbidity currents.

## 1. INTRODUCTION

OSCILLATORY boundary layer flows imply dynamic turbulence and possibly transition from laminar to turbulent flow. The interaction with an erodible bottom may give sand ripples and entrained sediments. Some of these features may be difficult to model. However, in the simplest special forms, oscillatory boundary layers offer the possibility to study dynamic flows without having to deal with dramatically new features (compare Telionis, 1981). For many years JONSSON's (1963) and JONSSON and CARLSEN's (1976) data on the mean velocity profile phase variations have been used as a common reference for model validation. Models based upon algebraic, few-equation and full Reynolds stress closures appear to predict these data accurately (FREDSØE, 1984; SHENG, 1984; HAGATUN and EIDSVIK, 1986; SUMMER *et al.*, 1987; DAVIES *et al.*, 1988; SHENG and VILLARET, 1989; JUSTESEN, 1991). Lately, data on turbulence characteristics have also become available (HINO *et al.*, 1983; SLEATH, 1987; JENSEN *et al.*, 1989; DICK and SLEATH, 1991). Since the mean velocity profile variations alone appear to be little model discriminant, the new data could hopefully contribute significantly to more critical model identification and thereby to increased understanding.

*SINTEF Norwegian Hydrotechnical Laboratory, N-7034 Trondheim, Norway.
†NTH Department of Structural Engineering, N-7034 Trondheim, Norway.

The present study addresses dynamic Reynolds stress modelling of oscillatory boundary layer flows. Since this and comparable models only describe the growth and decay of turbulence, not its initiation, the study is focused towards flows with large turbulent Reynolds number, $Re = |u_{*o}|\,\delta\nu \propto u^2_{*o}/\omega\nu \gg 1$. Here $|u_{*o}|$ and $\delta$ are the maximum friction velicity and boundary layer thickness respectively, $\delta \approx 0.5\,|u_{*o}|\,\omega^{-1}$. The oscillatory frequency and laminar kinematic viscosity coefficient are $\omega$ and $\nu$. Since we are most interested in the boundary layer flow below large ocean waves, the wave amplitude to surface roughness ratio is also supposed to be large, $a/z_o = u_o/\omega z_o \gg 1$. Here the free flow velocity amplitude is $u_o$ and the surface roughness is $z_o$.

It turns out that the Reynolds stress model predicts as realistically as the data allow us to decide. In this respect the study contributes to Reynolds stress model validation. From another point of view the study contributes to the understanding of why simpler models also predict oscillatory flow well. Based upon experience from turbidity currents (Brørs and Eidsvik, 1992) it is particularly unexpected that stably stratified sediment-laden oscillatory flows are predicted realistically by few-equation turbulence closures (Hagatun and Eidsvik, 1986). However, there are main differences between a turbidity and an oscillatory flow: (1) the oscillatory flow is strongly forced (by the pressure gradient) while the turbidity flow is forced by intricate interactions governed by the turbulence; and (2) the Reynolds stress model shows that the turbulence minimum within a turbidity flow is essential and requires sophisticated modelling. For an oscillatory flow the mean velocity extreme and the stress zero crossing are located near the top of the turbulent layer. Even if a few-equation model may predict the turbulence somewhat erroneously here, this is of minor importance.

On a slope, an oscillatory flow with sediment entrainment is predicted to force a systematic turbidity current. For such a situation, the Reynolds stress model is expected to be significantly more realistic than few-equation models (compare Brøs and Eidsvik, 1992). At sufficiently large slope angles, waves are predicted to trigger self-accelerated turbidity currents. This is consistent with the weak experimental evidence that is available (Pantin, 1986, and references therein).

## 2. MODEL

### 2.1. *First and second moment equations*

The flow is idealized to be a thin shear layer with insignificant along-flow gradients. The convective terms are assumed to be insignificant as compared to the time derivative terms. Standard Reynolds stress sediment modelling and notations are used (compare for instance Gibson and Launder, 1977 and Launder, 1989). The volume concentration of sediments, $c$, is supposed to be so small that the simplest two-phase models can be applied. The density and mass averaged horizontal velocity are given by $\rho = (1-c)\rho_f + c\rho_s$ and $\rho u_i = (1-c)\rho_f u_{fi} + c\rho_s u_{si}$. Here the density and velocity of the pure fluid and sediment components are $(\rho_f, u_{fi})$ and $(\rho_s, u_{si})$ respectively. The equations for the first two moments are then

$$\frac{\partial\langle\rho\rangle\,\langle u_i\rangle}{\partial t} = \frac{-\partial\langle p\rangle}{\partial x_i} + (\rho_s - \rho_f)\,\langle c\rangle\,g_i + \frac{\partial}{\partial x_k}\tau_{ik} \tag{1}$$

$$\frac{\partial\langle u_i' u_j'\rangle}{\partial t} = P_{ij} + G_{ij} + \phi_{ij} - 2\varepsilon\delta_{ij} + d_{ij} \tag{2}$$

$$\frac{\partial \varepsilon}{\partial t} = \left(C_{\varepsilon 1} \frac{1}{2} P_{ii} + C_{\varepsilon 3} \frac{1}{2} G_{ii} - C_{\varepsilon 2} \varepsilon\right) T_s^{-1} + d_\varepsilon \tag{3}$$

$$\frac{\partial \langle c \rangle}{\partial t} = \frac{\partial}{\partial x_k} (\langle c \rangle\, w_s \delta_{k3} - \langle c' u_k' \rangle) \tag{4}$$

$$\frac{\partial \langle u_i c \rangle}{\partial t} = P_{ic} + G_{ic} + \phi_{ic} + d_{ic} \tag{5}$$

$$\frac{\partial \langle c'^2 \rangle}{\partial t} = P_{cc} - \varepsilon_{cc} + d_{cc}. \tag{6}$$

The cartesian coordinate system is oriented along the alongflow, $x_1$, and normal coordinate, $x_3$. The gravitational acceleration and the sediment fall velocity are $g_i = g(\sin\beta, 0, -\cos\beta)$ and $w_s$. Even if the present flow is supposed to be a thin shear layer, general notations are convenient. However, more special notations may also be used: $x_1 \to x$, $x_3 \to z$, $u_1 \to u$, $u_3 \to w$, $\tau_{i3} \to \tau$. Except for the density and stress influence, two-phase effects upon the turbulence are neglected. The different turbulence terms in equations (1)–(6) are then given by $\tau_{i3} = -\langle \rho \rangle \langle u_i' u_3' \rangle - (\rho_s - \rho_f) \langle c' u_i' u_3' \rangle + \rho_s w_s \langle c \rangle \langle u_i \rangle$, $P_{ij} = -(\langle c_i' u_k' \rangle\, \partial \langle u_j \rangle / \partial x_k + \langle u_j' u_k' \rangle\, \partial \langle u_i \rangle / \partial x_k)$, $G_{ij} = \langle \rho \rangle^{-1} (\rho_s - \rho_f) (\langle c' u_j' \rangle g_i + \langle c' u_i' \rangle g_j)$, $\Phi_{ij} = \langle \rho \rangle^{-1} \langle p' (\partial u_i' / \partial x_j + \partial u_j' / \partial x_i) \rangle$, $d_{ij} = -(\partial / \partial x_k)(\langle u_i' u_j' u_k' \rangle + \ldots)$, $P_{ic} = -(\langle u_i' u_k' \rangle\, \partial \langle c \rangle / \partial x_k + \langle c' u_k' \rangle\, \partial \langle u_i \rangle / \partial_x)$, $G_{ic} = \langle \rho \rangle^{-1} (\rho_s - \rho_f) \langle c'^2 \rangle g_i$, $\Phi_{ic} = \langle \rho \rangle^{-1} \langle p' \partial c' / \partial x_i \rangle$, $d_{ic} = -\partial / \partial x_k (\langle u_i' c' u_k' \rangle + \ldots)$, $P_{cc} = -2 \langle c' u_k' \rangle\, \partial \langle c \rangle / \partial x_k$, $d_{cc} = -\partial / \partial x_k (\langle c'^2 u_k' \rangle + \ldots)$.

Turbulent closures are needed for the dissipation ($\varepsilon, \varepsilon_{cc}$), pressure correlations ($\Phi_{ij}$, $\Phi_{ic}$) and third moments in ($\tau_{i3}$, $d_{ij}$, $d_\varepsilon$, $d_{ic}$, $d_{cc}$). As already illustrated by the equations (1)–(6), the small-scale fluctuations are supposed to be isotropic and the turbulent dissipation $\varepsilon$ is identical to the energy transfer from the energy containing eddies, modelled by the *ad hoc* closure (3). The time scale for the down-scale energy transfer and the diffusive time scale are proportional to $T_s = 1/2\, \langle u_i'^2 \rangle / \varepsilon = k/\varepsilon$. The dissipation of concentration variance is approximated from the standard relation $\varepsilon_{cc} = 1/2 \langle c'^2 \rangle / R T_s$. With conventional Boussinesq modelling and the experimental relation $\langle u_i' c' \rangle \approx 2.0 \langle c' u_3' \rangle \cos\theta_i$, $i = 1, 2$, $\theta_i = \text{atn}\,(\langle u_i \rangle / \langle u_{j \neq i} \rangle)$ (LAUNDER, 1975), the turbulent stress is approximated in equation (7). As expected, it turns out that the first term on the right hand side dominates, but close to the bottom the last term may also be significant (BRØRS, 1991).

$$\tau_{i3} = -\langle \rho \rangle \langle u_i' u_3' \rangle + 2.0 (\rho_s - \rho_f) \cos\theta_i w_s^2 \langle c \rangle + \rho_s w_s \langle c \rangle \langle u_i \rangle. \tag{7}$$

The third moment diffusive terms are modelled by Boussinesq closures

$$\begin{aligned} d_{ij} &= C_s \frac{\partial}{\partial x_k} T_s \langle u_k' u_l' \rangle \frac{\partial \langle u_i' u_j' \rangle}{\partial x_l} \\ d_\varepsilon &= C_\varepsilon \frac{\partial}{\partial x_k} T_s \langle u_k' u_l' \rangle \frac{\partial \varepsilon}{\partial x_l} \\ d_{ic} &= C_{cs} \frac{\partial}{\partial x_k} T_s \langle u_k' u_l' \rangle \frac{\partial \langle c' u_i' \rangle}{\partial x_l} \\ d_{cc} &= C_c \frac{\partial}{\partial x_k} T_s \langle u_k' u_l' \rangle \frac{\partial \langle c'^2 \rangle}{\partial x_l}. \end{aligned} \tag{8}$$

The more controversial, non-observable pressure correlation terms are, as usual, divided into the sum of a slow turbulent, rapid mean strain and buoyant part as $\Phi_{ij} = \Phi_{ij1} + \Phi_{ij2} + \Phi_{ij3}$, $\Phi_{ic} = \Phi_{ic1} + \Phi_{ic2} + \Phi_{ic3}$. The slow turbulent part is modelled as Rotta's (1951) return to isotropy relation (9). The rapid strain part is modelled as the isotropisation of production model (IPM) in equation (10) (Launder, 1989). The buoyant term is modelled analogous to the (IPM)-expressions in equation (11).

$$\Phi_{ij1} = -\frac{C_1}{T_s}(\langle u_i'u_j'\rangle - \frac{2}{3}k\delta_{ij}), \qquad \Phi_{ic1} = -\frac{C_{c1}}{T_s}\langle c'u_i'\rangle \tag{9}$$

$$\Phi_{ij2} = -C_2\left(P_{ij} - \frac{1}{3}P_{kk}\delta_{ij}\right), \qquad \Phi_{ic2} = -C_{c2}\langle c'u_k'\rangle\,\partial\langle u_i\rangle/\partial x_k \tag{10}$$

$$\Phi_{ij3} = -C_3\left(G_{ij} - \frac{1}{3}G_{kk}\delta_{ij}\right), \qquad \Phi_{ic3} = -C_{c3}G_{ic}. \tag{11}$$

Wall modification of the pressure correlations are modelled by additive correction terms as described by Gibson and Launder (1977). Sediment–flow interactions are supposed to be unimportant for the turbulence except through the density and stress. No small Reynolds number corrections are applied. Although experience with this kind of modelling and standard coefficients may not always be fully consistent with all data, a standard coefficient vector is chosen: $(C_s, C_{cs}, C_c, C_\varepsilon, C_{\varepsilon1}, C_{\varepsilon2}, C_{\varepsilon3}, R, C_1, C_2, C_3, C_{c1}, C_{c2}, C_{c3}) =$ 0.22, 0.15, 0.11, 0.18, 1.45, 1.90, 1.45, 0.52, 1.8, 0.6, 0.5, 3.0, 0.5, 0.5) (Gibson and Launder, 1977).

The boundary conditions are chosen to be standard. At the upper boundary zero flux conditions are applied for all variables except for the Reynolds shear stress, which is set equal to zero. Since the lowest grid is located very close to the bottom, standard neutrally buoyant equilibrium relations are applied at the lower boundary. The bottom interaction is modelled by means of the boundary condition for $\langle c\rangle$ and $\langle c'u'_3\rangle$. For the purpose of comparison with simpler models, the $\langle c\rangle$-condition is kept unchanged (Hagatun and Eidsvik, 1986): $\langle c(0)\rangle = \max(c^1, c^2)$. Here $c^1 \le 0.3$ is approximated from Engelund and Fredsøe (1976) and $c^2$ is the bottom concentration for sediment settling in laminar flow. Concentration second moment gradients are specified as zero. The wall stress is obtained from the logarithmic velocity profile. Alternatively a zero gradient condition is applied for the shear stress. The normal stress components are specified from the friction velocity $|u_*|$; $|u_*|^2 = |\tau_{i3}(0)|/\rho(0)$ as given by Gibson and Launder (1977). For neutrally buoyant flows, these conditions contract to the set $\langle u_i^2\rangle/|u_*|^2 \approx (4.5, 2.6, 1.0)$. Concentration second moment gradients are specified as zero flux.

The forcing is provided by the oscillatory pressure gradient and gravitational effects. For a sinusoidal free flow, $\langle u(z\rangle\delta)\rangle = u_0 \sin\omega t$, the pressure gradient is specified to be independent of $x_3$ as

$$\partial\langle p\rangle/\partial x_1 = -\rho_f u_0 \omega^{-1}\cos\omega t. \tag{12}$$

## 2.2. *Integrations*

The integration scheme is implicit in time and central in the vertical coordinate. The vertical grid is equispaced on a logarithmic scale near the bottom. Without sediments *ca*

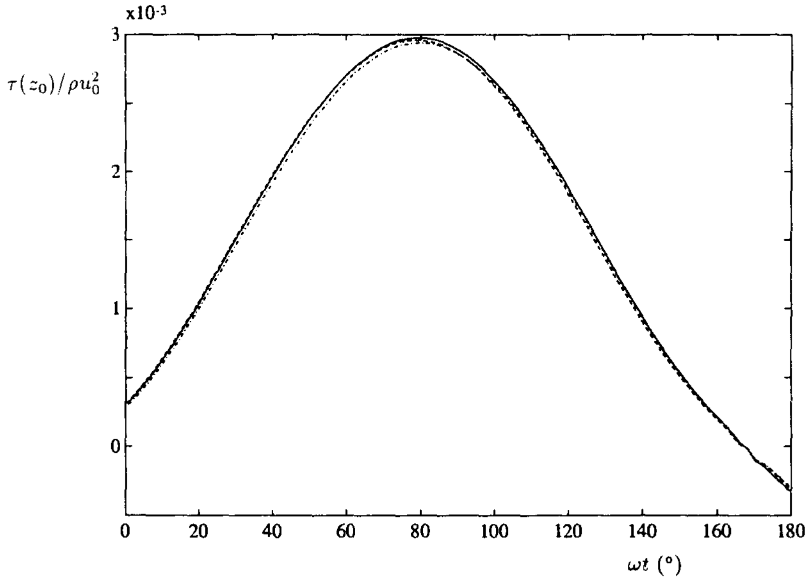


Fig. 1. Predicted bottom stress variations with phase for varying time steps. Flow corresponding to JENSEN *et al.* (1989). Run 13: $(T, u_0, z_0) = (9.72, 2.00, 3 \times 10^{-4})$ SI-units. 70 vertical grids. --- $\Delta t = 6 \times 10^{-3}$ s; —— $\Delta t = 1.3 \times 10^{-2}$ s; -·- $\Delta t = 1.7 \times 10^{-2}$ s.

70 grid points are necessary to obtain grid independent integrations. It turns out that the stress model tends to behave illconditioned as the near bottom layer flow changes direction. While a time step of *ca.* $\Delta t \approx T/200$ is sufficient to obtain periodic and reasonable integrations with a $(k\text{-}\varepsilon)$ model, it turns out that a significantly smaller value is necessary for the stress model. Even for $\Delta t < T/600$, small irregularities can be noticed as the bottom stress passes the zero value from the positive side (see Fig. 1). However, on the whole, the integrations are well defined when $\Delta t < T/600$.

## 3. DATA COMPARISON

Almost certainly, in a large model like this, there exists a coefficient adjustment that would give detailed fit to the available data. In this case the result of the analysis would be data representation, not model verification. It is important that a non-adjusted standard model, with commonly accepted coefficients, is compared to the data. As for other turbulent flows, when the relative difference between the prediction and data is less than about 20%, the estimates are judged to be as accurate as possible.

### 3.1. *Profiles*

JENSEN *et al.*'s (1989) experiments number 12 and 13 are associated with large *Re*- and $a/z_0$-numbers, and are complete in terms of turbulence data. These experiments are therefore chosen for detailed model comparison. The experimental characteristics for these runs are: $(T, u_0, z_0 = k_s/30) = (9.72, 1.02, 3 \times 10^{-4})$ and $(9.72, 2.0, 3 \times 10^{-4})$ SI-units. The distance from the bottom to the channel centre is $H = 0.14$ m. Because the roof of the channel is smooth, the shear stress at the rough bottom boundary is higher than at the top. This will presumably result in an asymmetric channel flow with a level of zero shear stress situated somewhere above the centreline level. For computational purposes, it is convenient to treat the upper boundary as a symmetry line. So, instead of prescribing wall boundary conditions at the top, it is assumed that the roof acts as a fictitious rough boundary 0.4 m above the bottom, and the upper computational boundary is placed in a symmetrical line $H = 0.2$ m away from the bottom. This height is consistent with a ratio of smooth roof to rough bottom shear stress of about 3/4, which seems reasonable in view of Jensen *et al.*'s (1989) shear stress measurements for smooth and rough boundaries. The maximum friction velocity is approximately $u_{*0} = 0.058$ for Run 12 and $u_{*0} = 0.11$ for Run 13 (Jensen *et al.*, 1989) and turbulent Reynolds- and amplitude to roughness numbers ($Re = u_{*0}^2/\omega\nu$, $a/z_o$) are ($5 \times 10^3$, $6 \times 10^4$) and ($2 \times 10^4$, $1 \times 10^5$) for the two runs. In Run 12, corresponding to the smallest Reynolds number, the flow may not be fully developed turbulent at all phases (Jensen *et al.*, 1989). Nevertheless, as illustrated by Figs 2 and 3, the data and predictions show excellent agreement for both experiments.

The phase variations of an oscillatory flow are well characterized relative to the level of vanishing stress, $\tau = 0$, which is almost the same as the level of mean velocity maximum and a minimum or inflection point of the normal velocity variance components. The bottom stress lead relative to the free current is consistent with common experience. From the phase value where $\tau = 0$ at $z = 0$, the level with $\tau = 0$ rises approximately linearly with phase both during the accelerating and decelerating stages. Below this level the acceleration stage is characterized by increasing wall extrema of all second moments. During the deceleration stage the low level phase lead implies that the extrema are lifted away from the bottom to become secondary extrema for the next wave, with opposite mean velocity and shear direction. This picture, containing the main features of the shape of the profiles in Figs 2 and 3, is predicted and measured almost identically.

The magnitude of the signals are also realistically predicted, particularly so for the mean velocity and shear stress. However, there appears to be some discrepancy between the predictions and data in the decelerating stage before zero crossing. Here the mean velocity is predicted to be slightly too large and the stress slightly too small. The normal stress components are most accurately predicted near phase angles of $\pi/4$. Here the secondary turbulent kinetic energy maximum is accurately predicted as *ca.* 0.45 times the near wall maximum (Summer *et al.*, 1987). Justesen's (1991) ($k$-$\varepsilon$) model predicts this ratio to be *ca* 0.25. Although the latter prediction is also fairly accurate, it appears as the present model predicts the upper layer variations somewhat better. The predictions and data are different on the magnitude of the normal stress components at the upper layers, near phase shifts. However, this may not imply model deficiency. Since the measured magnitude of the normal stress components at these levels are almost phase independent, with no shear stress, it could be that there is 'background turbulence' in the flume.

### 3.2. *Characteristic variables; phase variation*

To focus upon the main features of the predicted flow fields, illustrated in Figs 2 and 3, the phase variations of the main flow characteristics ($u_m$, $\delta$, $\tau(0)$, $\delta^*$) are illustrated in Fig. 4. The characteristics are: magnitude and height of the mean velocity maximum, wall stress and height to the level of zero stress.

As illustrated in Fig. 4(a) the phase variation of $\delta(\omega t)$ is almost linear. Over the phase interval where the mean velocity maximum is well defined, there is a definite similarity

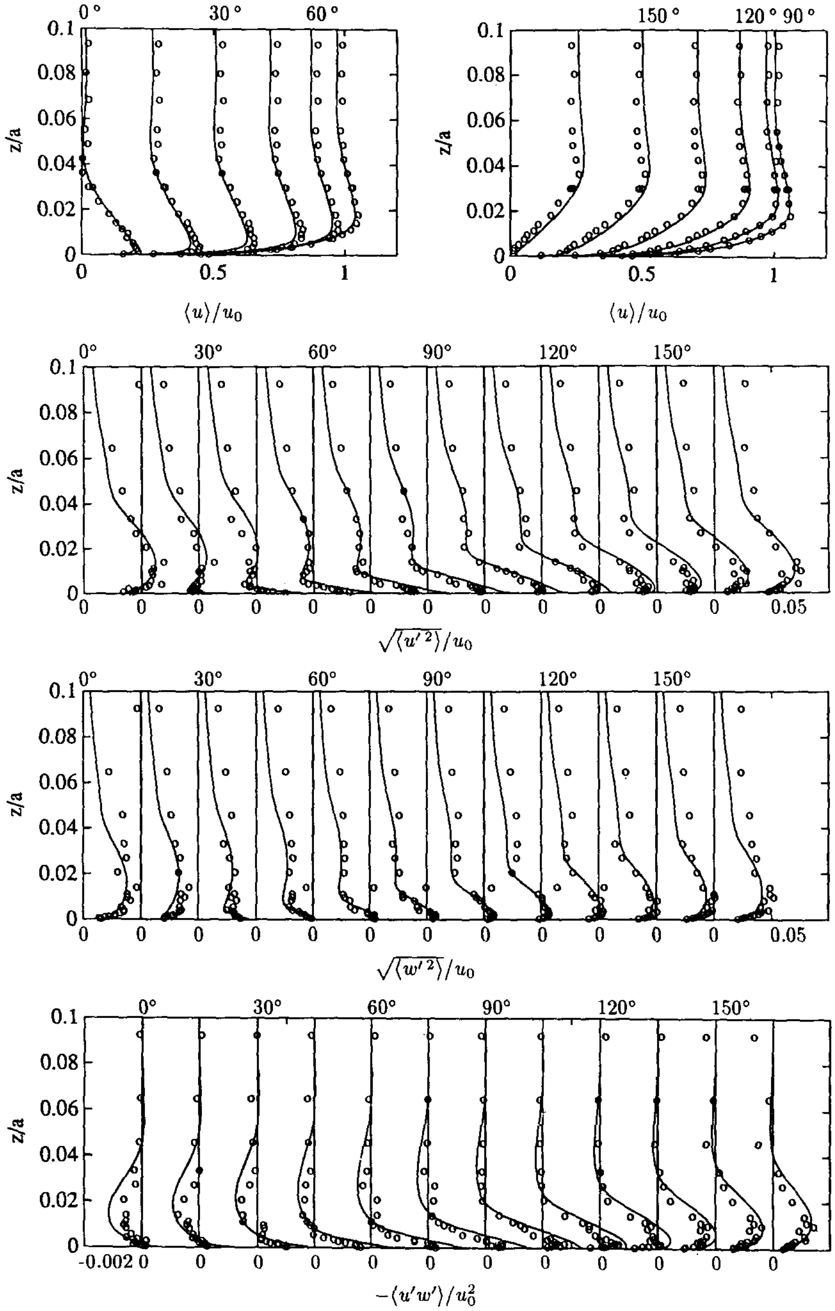


Fig. 2. Oscillatory channel flow. Predicted and observed profiles at phase angles ranging from 0 to 165° in steps of 15°. Fixed origin for accelerating and decellerating mean velocity profiles. For other variables the origin and curves are moved to the right as the phase increases. Circles: Data from JENSEN *et al.* (1989). Run 12: $(T, u_o, z_o) = (9.72, 1.02, 3 \times 10^{-4})$ SI-units.

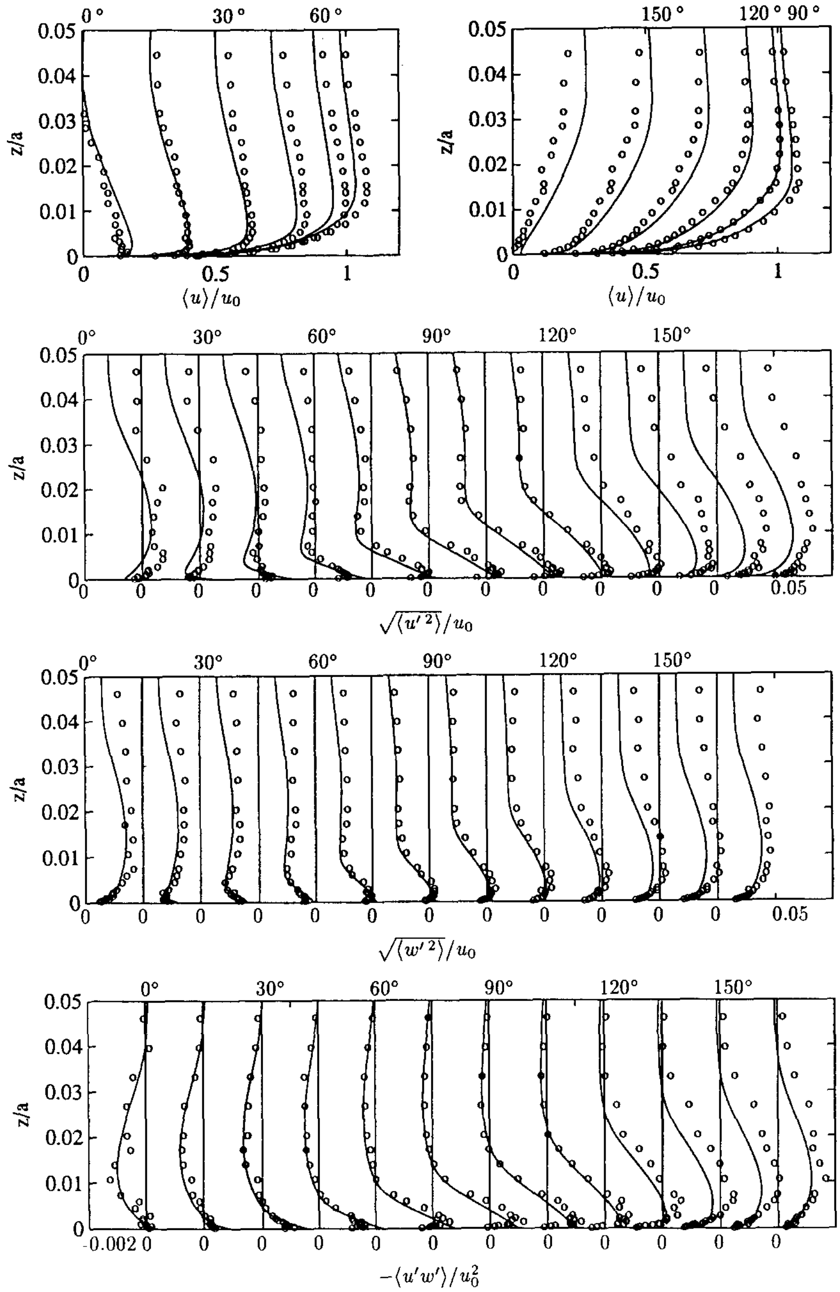


Fig. 3. As in Fig. 2. Run 13: $(T, u_0, z_0) = (9.72, 2.00, 3 \times 10^{-4})$ SI-units.

between predicted and measured values. Near the end of the decellerating period, where the mean velocity maximum is expanded (compare Figs 2 and 3), the uncertainty in estimated $\delta$-values must be larger and the discrepancy between measured and predicted values may not be significant. The normalized mean velocity maximum is illustrated in Fig.

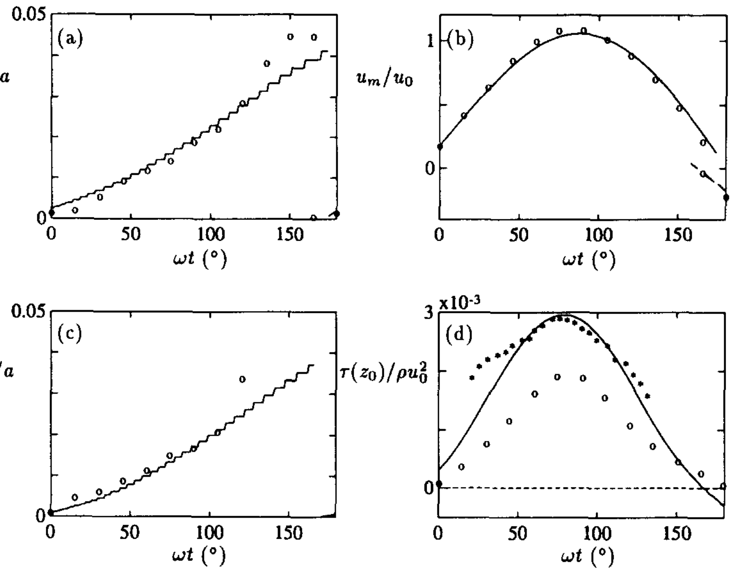


Fig. 4. Phase-dependency of boundary layer parameters predicted and measured. Circles: Data from JENSEN *et al.* (1989) Run 13. In diagram (d), circles represent bottom stress from direct measurements of $\langle u'v' \rangle$ and asterisks represent estimated bottom stress from fit to logarithmic velocity profile in their Fig. 7.

4(b). At all phases there is a remarkable similarity between predicted and measured values.

Turbulence characteristics are specified in terms of bottom shear stress and height to the level of zero shear stress. The latter is illustrated in Fig. 4(c), and again there is a good correspondence between the predictions and the data. Comparing Fig. 4(a) and (c) also show that the level of mean velocity maximum and the level of zero stress are almost similar, as they should if a Boussinesq turbulent viscosity closure were realistic. The predicted and measured bottom stress is focused in Fig. 4(d). There appears to be a significant difference between the bottom stress estimated from the mean velocity profile and from the turbulent fluctuations. However, it should be kept in mind that the relative stress error is about two times larger than that of the friction velocity. In terms of turbulent velocity the difference between the two estimates in Fig. 4(d) is therefore only *ca* 20%. The predicted maximum bottom stress is almost similar to the stress estimate based upon the mean velocity profile. The maximum bottom stress is much smaller than in a stationary channel flow with a pressure gradient equal to the present pressure gradient amplitude, $\tau_{p0} = \rho_f \omega^{-1} u_0 H$. While the predicted and measured bottom stress phase lead are comparable near stress maximum, they appear to differ slightly near zero crossings. With the LDA-data uncertainty in mind (JENSEN *et al.*, 1989), it is claimed that the bottom stress is predicted as accurately as the available data allow us to decide. Few-equation turbulence models also predict these features reasonably accurately (JUSTESEN, 1991).

### 3.3. *Bulk data comparison*

By varying the surface roughness, $z_0$, and thereby ($Re$, $a/z_0$), the predictions can be compared to most data. Figure 5(a) illustrates the predicted and measured boundary layer

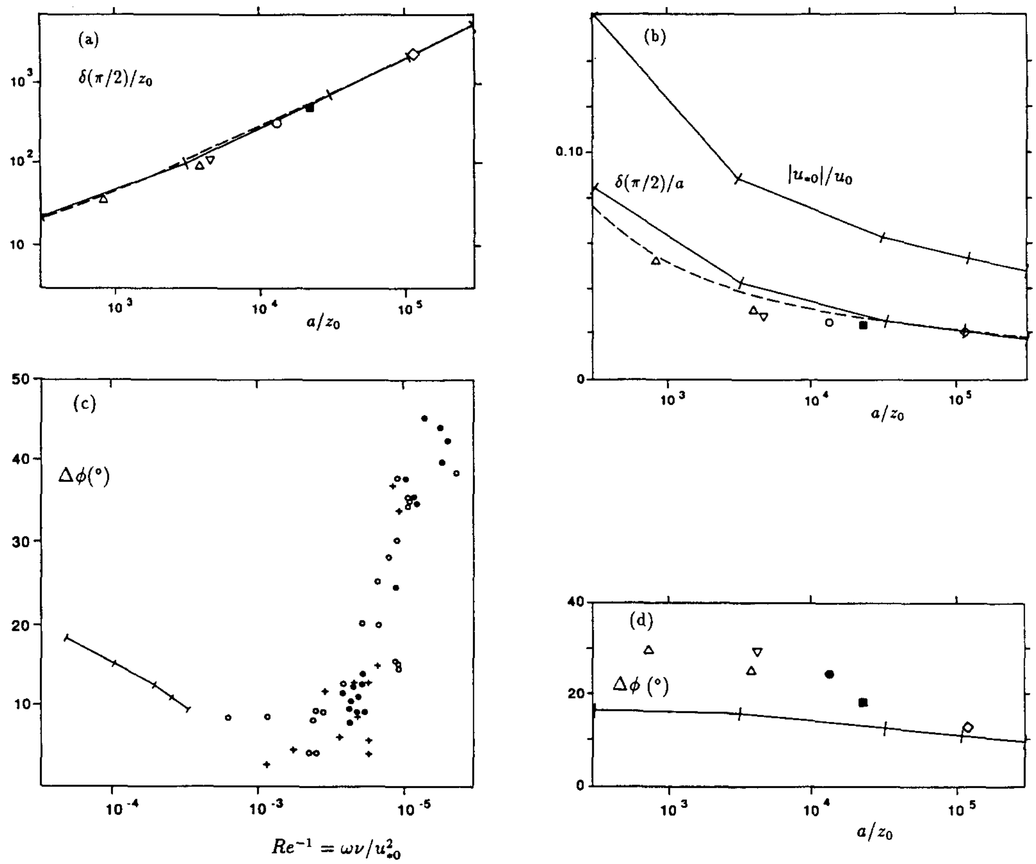


Fig. 5. Boundary layer characteristics. Predicted values by present model: ——+——. FREDSØE's (1984) prediction: - - - -. (a), (b) Boundary layer thickness. Data from JENSEN *et al.* (1989). (c) Bottom stress phase lead over free flow velocity. Data refered by COUSTEIX (1986). (d) Maximum bottom stress phase lead over maximum free stream velocity. Data from JENSEN *et al.* (1989).

thickness $\delta(\pi/2)/z_o$ as a function of wave amplitude $a/z_o$. The model predicts the data accurately, as FREDSØE's (1984) model also does. Figure 5(b) illustrates the boundary layer thickness as normalized with the wave amplitude, $\delta(\pi/2)/a$. The model predicts the data very well also from this point of view, as FREDSØE's (1984) model also does. In Fig. 5(b) the predicted normalized maximum friction velocity $|u_{*o}|/u_o$, is plotted as well ($|u_{*o}| = (\tau(0)_{max}/\langle\rho\rangle)^{1/2}$). The simulations suggest that $\delta(\pi/2)/a \propto |u_{*o}|/u_o$, with a fairly constant proportionality factor. This is consistent with common experimental estimates. In greater detail, the proportionality factor is predicted to decrease from about 0.5 to 0.4 over the interval $a/z_o \, \varepsilon \, (10^3, 10^5)$.

Figure 5(c) and (d) illustrates the bottom stress phase lead over the free stream velocity. The phase difference in Fig. 5(d) is based upon conditions near maximum free velocity [compare Fig. 4(d)]. Both for the predictions and the experiments referred to in Fig. 5(d), the Reynolds number is of the order of $Re = 0\,(3 \times 10^3, 2 \times 10^4)$. With the measurement uncertainty associated with the bottom stress taken into account, Fig. 5(d) is interpreted as a confirmation of model realism.

The data referred to by Cousteix (1986) in Fig. 5(c) are from small Reynolds number experiments. The smallest Reynolds number phase lead of about $\pi/4$ may be understood in terms of the classic Stokes solution with a constant laminar viscosity coefficient. At the largest Reynolds numbers the turbulence in the boundary layer is likely to be so vigorous that the turbulent viscosity coefficient varies little with height and phase. A simplified model based upon the Boussinesq viscosity assumption, will then be analogous to the laminar case with the laminar viscosity coefficient replaced by a fairly constant turbulent viscosity coefficient. Therefore the phase lead increases for the largest Reynolds numbers, and the minimum phase lead around Reynolds numbers of $Re = 0\ (10^3)$ suggested by Fig. 5(c) is reasonable. In this range transitions from laminar to turbulent flow will most probably be essential, and detailed modelling will be difficult.

### 3.4. *Sediment entrainment*

With sediment density, diameter and fall velocity $\rho_s = 2.6 \times 10^3$ kg m$^{-3}$, $d = 10^{-4}$ m, $w_s = 6 \times 10^{-3}$ m s$^{-1}$ and oscillatory flow characteristica $(u_o, T, z_0) = (1, 10, 10^{-5})$ SI-units, the predicted flow is illustrated in Fig. 6. Without sediments, the flow is predicted analogous to what is illustrated in Figs 2 and 3. With entrained sediments, a most significant change is that the boundary layer flow, with most turbulence, is closer to the bottom, with a more pronounced mean velocity maximum and phase lead. Except for phase angles near zero crossings, the turbulent stress is almost vanishing above the level where $\tau = 0$, and there is a pronounced minimum or reduction of the normal stress components near this level. Without sediments the maximum stress components are predicted at the bottom for smaller phase angles than about $\pi/2$. At larger phase angles this maximum is lifted into the flow. With sediments the low level maximum is predicted to be detached from the bottom at all phase angles except close to zero crossings (Fig. 6). However, the latter effect does not turn out to be dominant for sediments in a flow corresponding to Fig. 3. The maximum stress is slightly reduced with sediments. The sediment concentration characteristica are illustrated in Fig. 6(b). During the acceleration stage and maximum free stream velocity, sediments are entrained. However, the turbulent fluxes above the level where $\tau = 0$ are almost vanishing so that most of the entrained sediments are confined to lower layers.

The model is compared with Ribberink and Al-Salem's (1992) experiment C10 in Fig. 7. $(u_o, T_o, d, w_s, \rho_s) = (1.7, 7.2, 0.00021, 0.026, 2650)$ SI-units. $z_o = 0.08\ d$. Figure 7(a) illustrates the predicted height and phase variation of the expected sediments mass concentration, and Fig. 7(b) shows data comparisons. Since no model adjustment is done, we claim that the data are predicted as accurately as can be expected. The general height decrease is very accurately predicted, while the phase can be associated with errors. The phase lag between the low level sediment concentration and the free stream velocity is probably the most significant feature that is predicted and measured differently. However, the height variation of this phase lag is also predicted and estimated from the data differently. Figure 7(a) and (b) illustrate the predicted phase lag smoothly increasing with height. From the data it appears that the lag is almost constant below about 2 cm height. Between about 2 and 3.1 cm there is inconclusive information on this feature. Above about 3 cm the lag is again estimated to be fairly constant. Physically there cannot be a phase lag decrease with height of sediment concentration. This means that the data suggest a lag

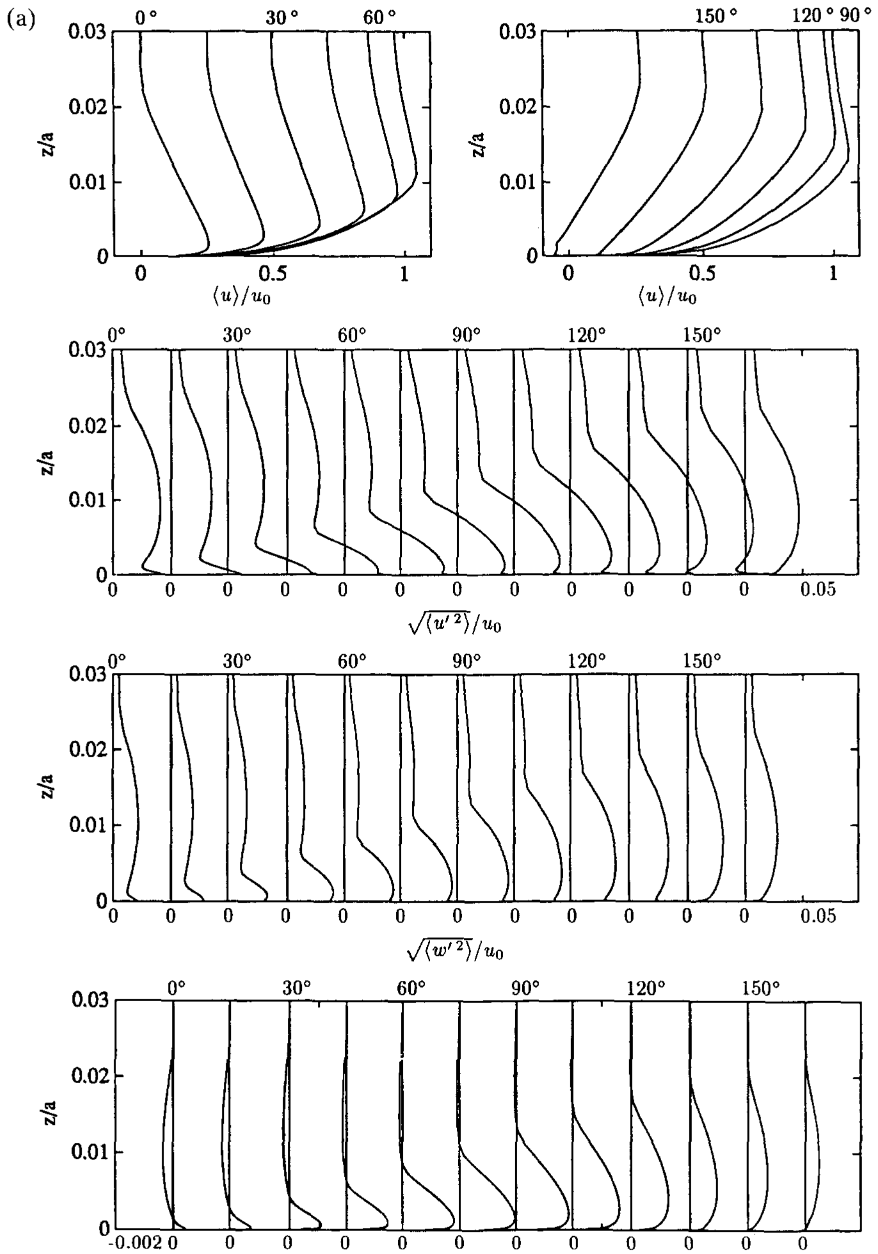


Fig. 6. (a). Predicted oscillatory flow with entrained sediments. $(u_0, T, z_0, d, w_s) = (1, 10, 10^{-}$ $10^{-4}, 6 \times 10^{-3})$ SI-units. Velocity characteristics.

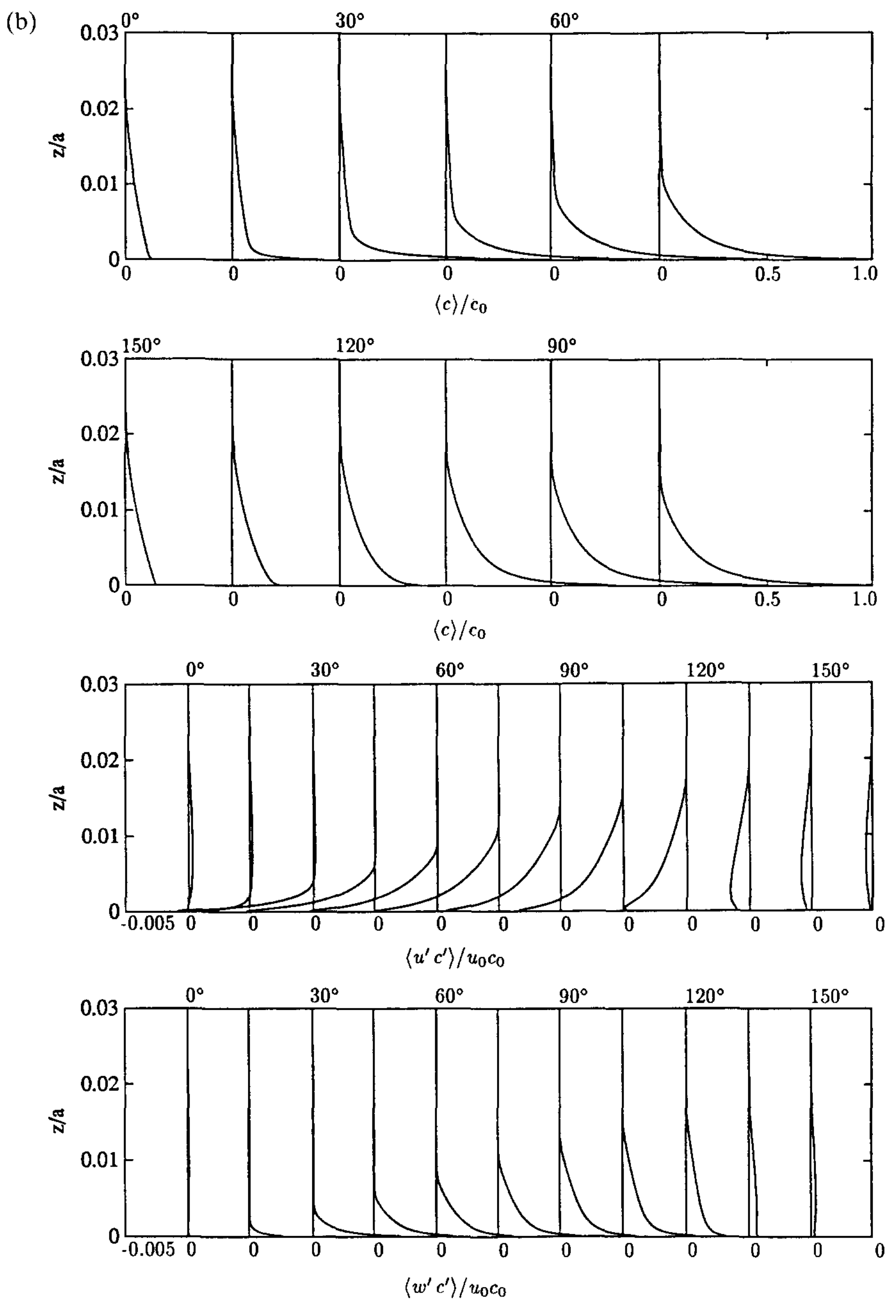


Fig. 6. (b). As in Fig. 6(a); sediment characteristics.

variation as large as about $\pi$ over the height interval from about 2 to 3 cm. Could it be that the phase information in the data is not as accurate as desirable?

Data on sediment-laden oscllatory flows have previously been compared favourably with a model based upon ($k$-$\varepsilon$) turbulence closure (HAGATUN and EIDSVIK, 1986; HAGA-

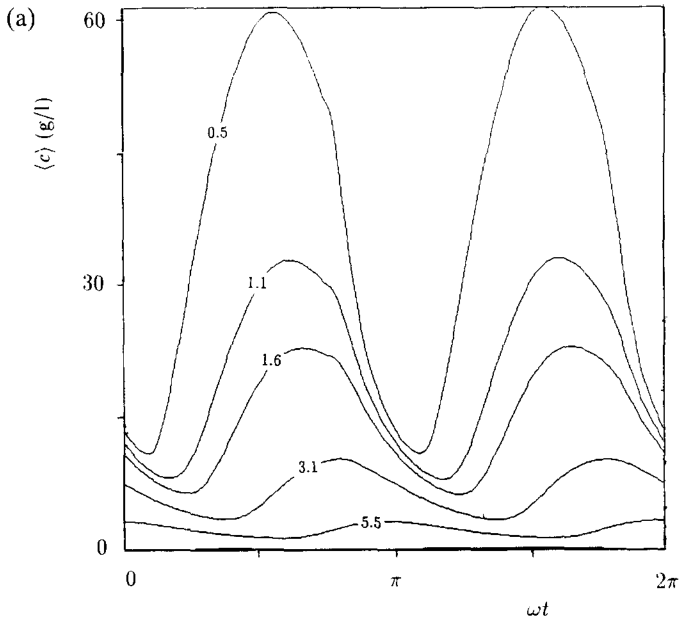


Fig. 7. (a). Predicted expected sediment mass concentration as varying with height and wave phase. $(u_0, T_0, d, w_s,) = (1.7, 7.2, 0.00021, 0.026)$ SI-units, $z = (0.5, 1.1, 1.6, 3.1, 5.5, 10)$ cm.

TUN, 1987). The data are probably so few and uncertain that they cannot identify a better model.

The present model predictions are compared with HAGATUN's (1987) ($k$-$\varepsilon$) predictions of sediment-laden flow in Fig. 8(a) and (b). Below the mean velocity maximum, the area with the most significant variations, there is a remarkable similarity between the two predictions. The limited discrepancy between the two models above this level, in for instance the turbulent length-scale, is not essential because the turbulence is very weak here. This similarity implies that the data comparisons with sediment-laden oscillatory flows previously done with a ($k$-$\varepsilon$) model (HAGATUN and EIDSVIK, 1986), can be applied to the full stress model. As far as common sense and scarse data allow us to decide, the sediment feature of the full stress model is therefore also reasonable.

From another point of view this implies that a simple ($k$-$\varepsilon$) model predicts oscillatory sediment-laden flows as realistically as a full Reynolds stress model (compare HAGATUN and EIDSVIK, 1986; SHENG and VILLARET, 1988). This may be surprising when compared to experience from turbidity currents (BRØRS and EIDSVIK, 1992). A reason could be that the data are so scarce, with so large uncertainty, that model errors are difficult to detect. However, a major error of ($k$-$\varepsilon$) models near levels of vanishing stress within the turbidity flow (BRØRS and EIDSVIK, 1992), is not essential for oscillatory flows. As illustrated by Fig. 8, the turbulent stress below the level where $\tau = 0$ is predicted to be almost similarly predicted by both models. Above this layer the turbulence is predicted to be weak. Even if the ($k$-$\varepsilon$) model may predict somewhat erroneously here, the exact magnitude of the turbulence quantities near the top of the turbulent boundary layer is not essential.

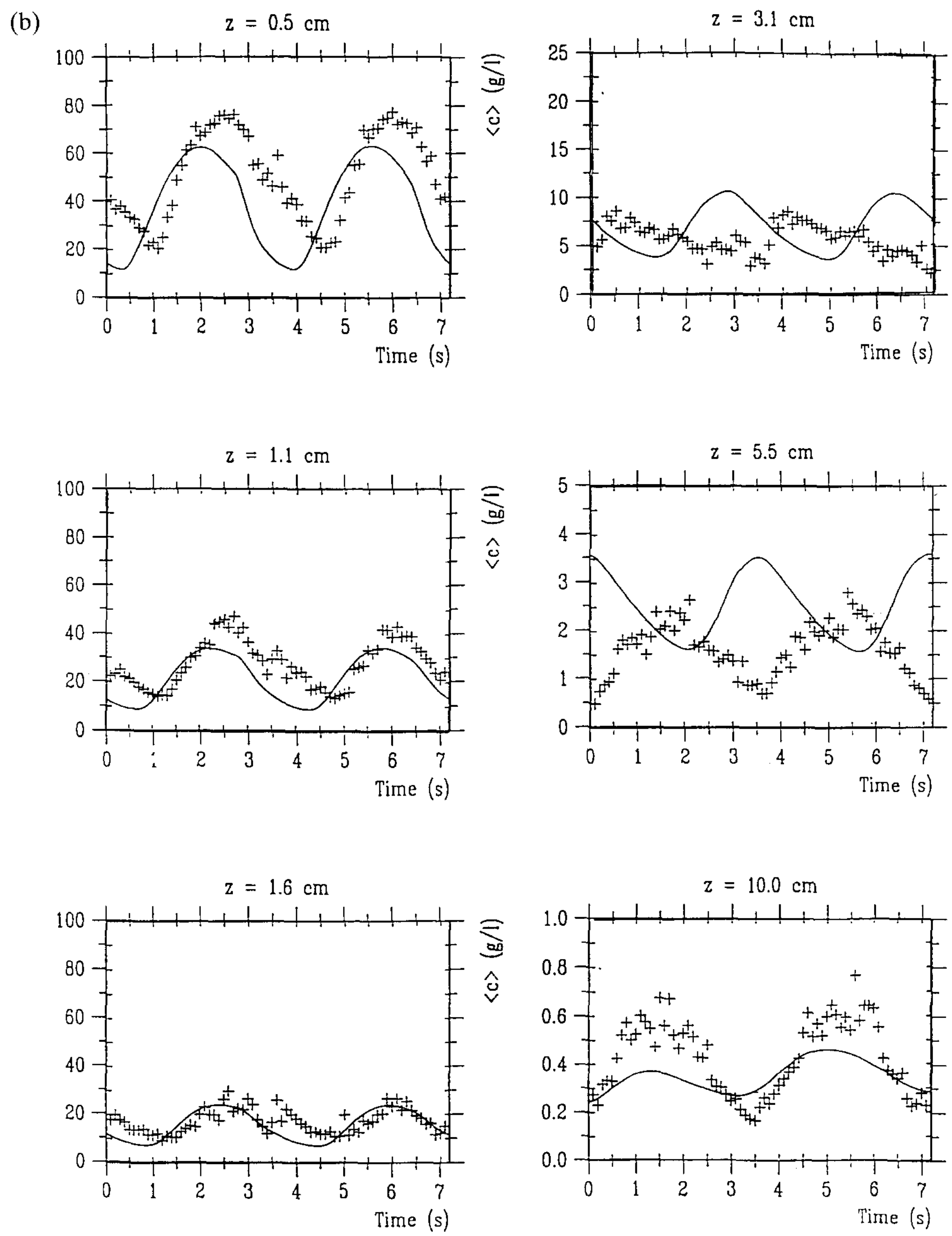


Fig. 7. (b). As in Fig. 7(a); expected sediment mass concentration as estimated from predictions and data. Data from Ribberink and Al-Salem (1992), experiment C10.

Another feature is that the oscillatory flow is strongly forced (by pressure gradient). It is not decisively governed and even forced by the turbulence, as is a self-ignitive turbidity flow.

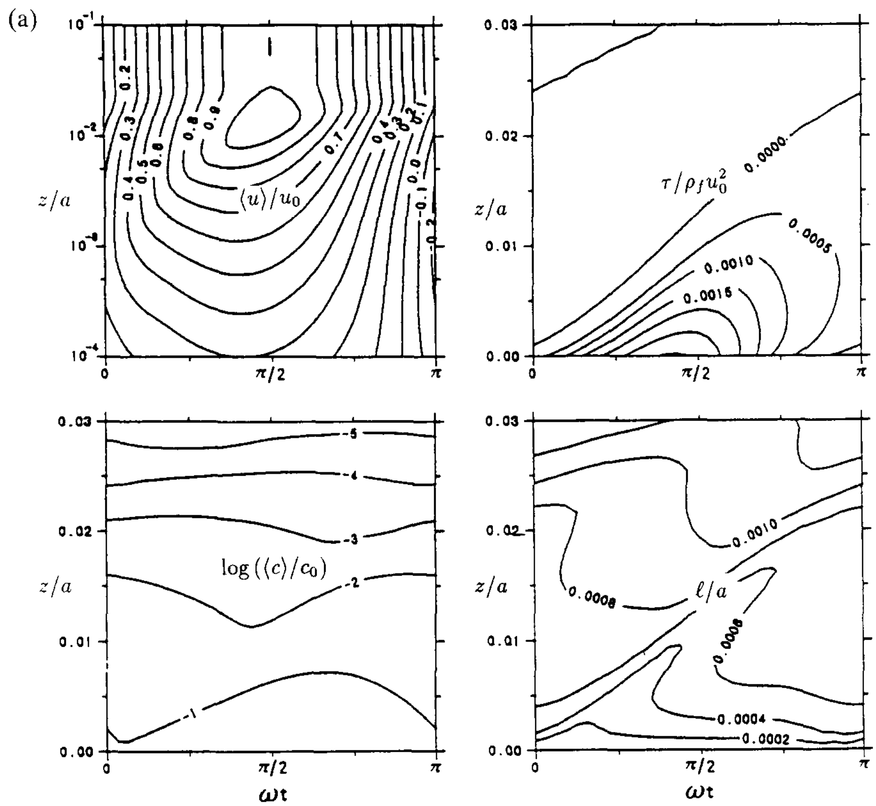


Fig. 8. (a). Sediment-laden oscillatory flow $(u_0, T, a_0, d, w_s) = (1, 10, 10^{-5}, 10^{-4}, 6 \times 10^{-3})$ SI-units. HAGATUN's (1987) ($k$-$\varepsilon$) predictions.

## 4. WAVE FORCED TURBIDITY CURRENT AND TRIGGERING OF SELF-IGNITIVE TURBIDITY FLOWS

Oscillatory flow with sediment entrainment on slopes may reasonably generate a systematic down-slope mean current. It is even believed that this may trigger avalanches (PANTIN, 1986). As opposed to simpler models, the present model is expected to describe turbidity flows realistically (BRØRS and EIDSVIK, 1992), so that its predictions on this subject should be of some interest.

The oscillatory flow is chosen as in Fig. 3, with sediments as in Fig. 8. Each integration is initiated smoothly from a periodic flow over flat bottom introducing the slope angle gradually. For small slope angles, it turns out that the oscillatory flow with suspended sediment forces a period average stationary downslope flow. Figure 9(a) illustrates the period average as well as maximum and minimum suspended sediment mass as a function of slope angle. For small slope angles the suspended mass is significantly smaller, $M = 0$ $(10^2$ kg m$^2)$, than the critical mass necessary for a self-ignitive turbidity flow, $M_c = 0$ $(10^2$ kg m$^2)$; (PANTIN, 1979; EIDSVIK and BRØRS, 1989). Figure 9(b) and (c) illustrate the stationary period average velocity and downslope sediment flux profiles as functions of the slope angle. Even on small slope angles, the waves force a systematic down-slope flow.

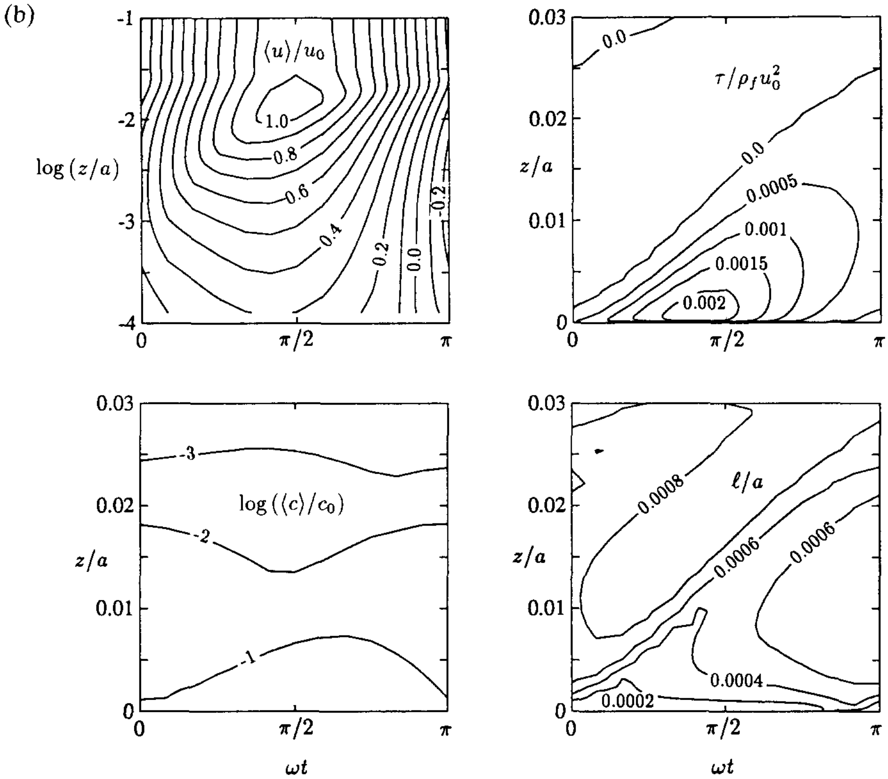


Fig. 8. (b). As in Figs 6(a) and 7(a); present model predictions.

Although the magnitude of the period average flow may be significantly smaller than the oscillatory amplitude, the average flow is systematic so that its sediment transport to deeper waters may be important.

For larger slope angles a stationary period average solution no longer exists. Figure 10(a) illustrates the time development of the suspended sediment mass and bottom stress for such a flow. During a few oscillations the critical mass of sediments is entrained and the flow develops into a self-ignitive turbidity current. It may be surprising that the bottom stress displays larger and larger amplitude, with small values near pressure gradient minima. However, the instantaneous profiles appear reasonable. It should be kept in mind that the turbidity flow is shallow, with purely oscillatory flow above. This means large mean velocity shear near the free stream velocity minima. The time developments of the period average velocity and downslope sediment flux are illustrated in Fig. 10(b) and (c). During a few oscillations the turbidity flow is significantly stronger and deeper than the oscillatory boundary layer flow, and the average flow resembles the structure of a pure turbidity flow (Brørs and Eidsvik, 1992).

The wave and sediment characteristica chosen for the predictions are not extreme. Still the model predicts that the waves may trigger avalanches on slopes with as small inclination as *ca* 8°. Once it is generated, an avalanche may continue to develop on slopes with inclinations as small as about 1° (Brørs and Eidsvik, 1992). Since the present model is

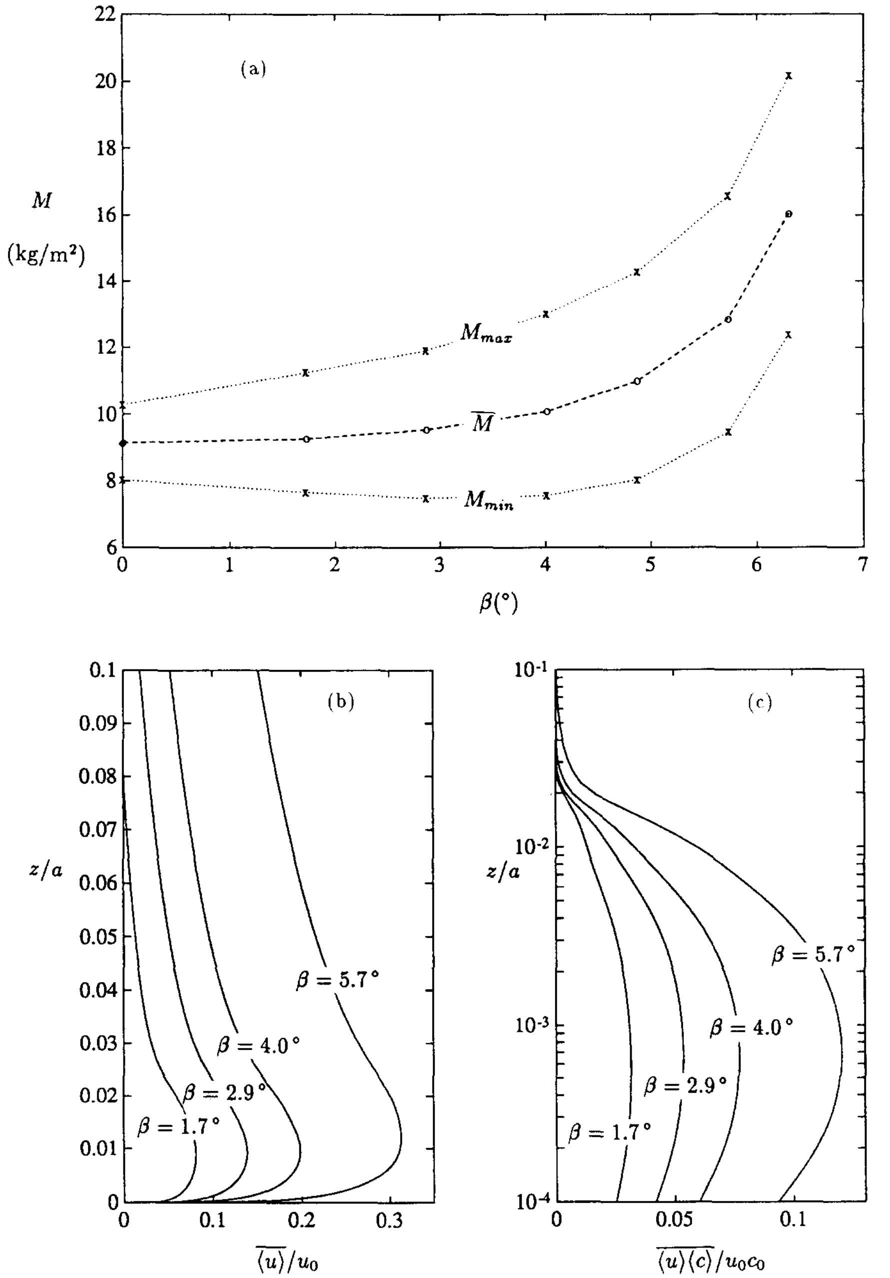


Fig. 9. Oscillatory flow as in Fig. 3 with sediments as in Fig. 8, on slopes. Stationary period average characteristics. (a) Suspended sediment mass. (b) Velocity profile. (c) Downslope sediment flux.

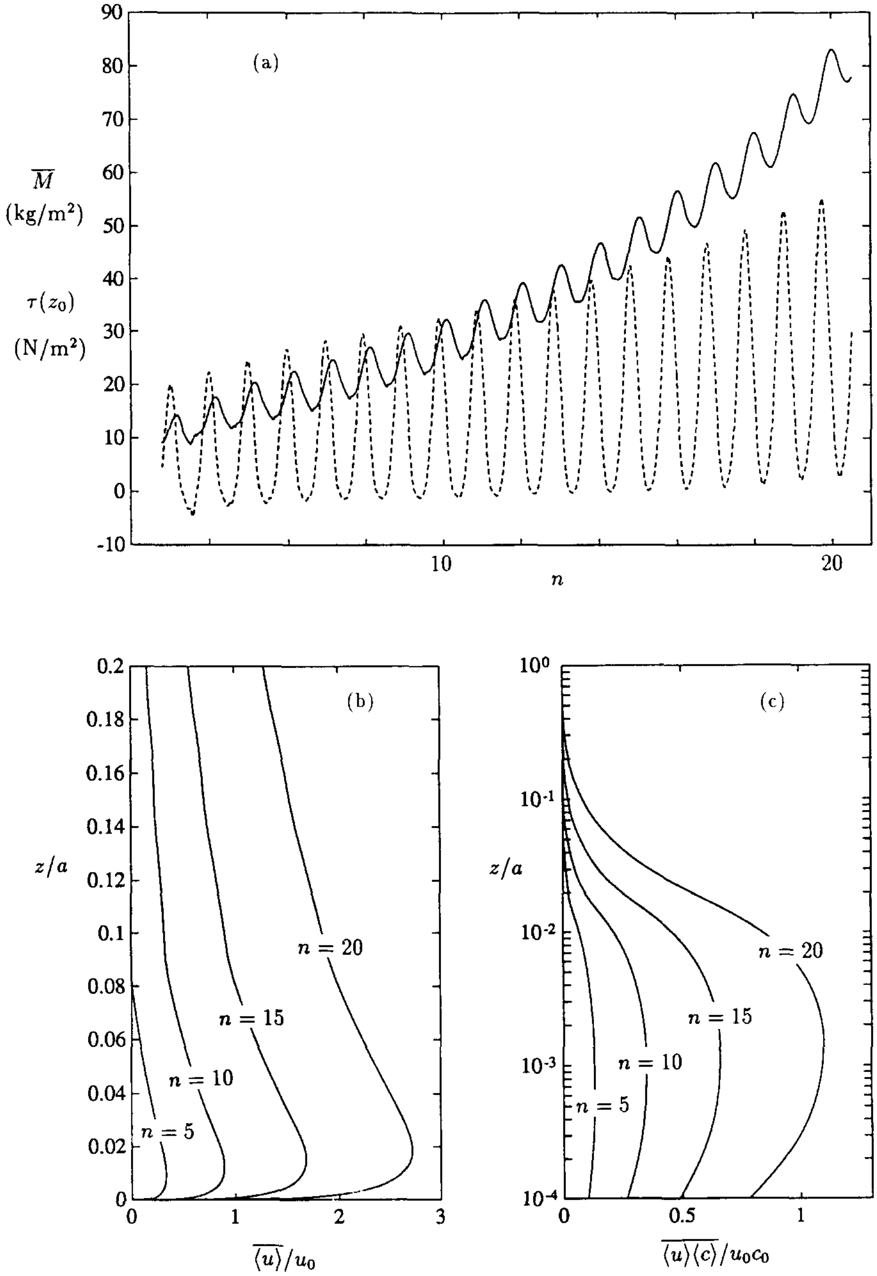


Fig. 10. As in Fig. 9. Slope angle $\beta = 8.6°$. Wave triggered self-ignitive turbidity flow. (a) Time development of suspended sediment mass (full line) and bottom stress (dashed line). (b) Time development of period average velocity profile. (c) Time development of period average down-slope sediment flux.

generally validated, and in particular validated relative to data from turbidity and oscillatory flows, its predictions on these points are significant. This prediction also appears to be consistent with the weak experimental evidence that is available (PANTIN, 1986 with references therein).

## 5. CONCLUDING REMARKS

A model based upon full Reynolds stress closure is applied to oscillatory boundary layer flow. The model is not as robust as few equation models are. However, when the boundary layer thickness and period are resolved by vertical grid and timestep numbers of the order of 100 and 600 respectively, well defined integrations are obtained.

High Reynolds number data (JENSEN *et al.*, 1989) are predicted to great detail. Even secondary extrema of the stress components above the mean velocity maximum are fairly well predicted. Variations of boundary layer thickness and bottom stress amplitude and phase lead are realistically predicted as compared to several data sources referred to by JENSEN *et al.* (1989) and COUSTEIX (1989). With sediments eroded from the bottom, the model compares well with predictions by a ($k$-$\varepsilon$) model, and therefore also compares well with the scarce data from such flows (HAGATUN and EIDSVIK, 1986).

The oscillatory boundary layer data contribute towards verifying the realism of dynamic Reynolds stress models. However, even with turbulence characteristica, such data do not appear to be very model discriminant. The much simpler, standard ($k$-$\varepsilon$) model also predicts these data reasonably realistically. It may be unexpected that the ($k$-$\varepsilon$) model even appears to predict stratified sediment-laden flows fairly accurate. In other types of stratified flows, simple models of this type predict the turbulence near a mean velocity extremum significantly in error (compare BRØRS and EIDSVIK, 1992). For the present sediment-laden flow the turbulence above this layer is predicted to be vanishingly small in both models. Even if the ($k$-$\varepsilon$) model may predict somewhat erroneously here, this is not essential. Also the oscillatory flow is strongly forced (by the pressure gradient), while the turbidity current is forced by intricate interactions governed by the turbulence.

On a slope, waves with sediment entrainment are predicted to force systematic down-slope flows. At larger slope angles the waves may even trigger self-ignitive turbidity flows.

*Acknowledgements*—The study was supported by fellowships from NTNF and Statoil.

## REFERENCES

BRØRS B. (1991) Turbidity current modelling. Dr. Ing. thesis, The University of Trondheim, 164 pp.

BRØRS B. and K. J. EIDSVIK (1992) Dynamic Reynolds stress modelling of turbidity currents. *Journal of Geophysical Research*, **97**(C6), 9645–9652.

COUSTEIX J. (1986) Three-dimensional and unsteady boundary layer computations. *Annual Review of Fluid Mechanics*, **18**, 173–196.

DAVIES A. G., R. L. SOULSBY and H. L. KING (1988) A numerical model of the combined wave and current bottom boundary layer. *Journal of Geophysical Research*, **93(C1)**, 491–508.

DICK E. J. and J. F. A. SLEATH (1991) Velocities and concentrations in oscillatory flow over beds of sediment. *Journal of Fluid Mechanics*, **233**, 165–196.

EIDSVIK K. and B. BRØRS (1989) Self-accelerated turbidity current prediction based upon ($k$-$\varepsilon$) turbulence. *Continental Shelf Research*, **9**, 617–627.

ENGELUND F. and J. FREDSØE (1976) A sediment transport model for straight alluvial channels. *Nordic Hydrology*, **7**, 293–306.

FREDSØE J. (1984) Turbulent boundary layer in wave-current motion. *Journal of Hydraulic Engineering, ASCE*, **110(8)**, 1103–1120.

GIBSON M. M. and B. E. LAUNDER (1977) Ground effects on pressure fluctuations in the atmospheric boundary layer. *Journal of Fluid Mechanics*, **86**, 491–511.

HAGATUN K. and K. J. EIDSVIK (1986) Oscillating turbulent boundary layer with suspended sediments. *Journal of Geophysical Research*, **91**(C11), 13,045–13,055.

HAGATUN K. (1987) A model for oscillatory turbulent boundary layers with suspended sediment. Dr. Ing. thesis, The University of Trondheim, 99 pp.

HINO M., M. KASHIWAYANAGI, A. NAKAYAMA and T. HARA (1983) Experiments on the turbulence statistics and the structure of a reciprocating oscillatory flow. *Journal of Fluid Mechanics*, **131**, 363–400.

JENSEN B. L., B. M. SUMER and J. FREDSØE (1989) Turbulent oscillatory boundary layers at high Reynolds numbers. *Journal of Fluid Mechanics*, **206**, 265–297.

JONSSON I. G. (1963) *Measurements in the turbulent wave boundary layer*. Proceedings of the 10th Congress, IAHR, London, **1**, 85–92.

JONSSON I. G. and N. A. CARLSEN (1976) Experimental and theoretical investigations in an oscillatory turbulent boundary layer. *Journal of Hydraulic Research*, **14**, 45–60.

JUSTESEN P. (1991) A note on turbulence calculations in the wave boundary layer. *Journal of Hydraulic Research*, **29**(5), 699–711.

LAUNDER B. E. (1975) Heat and mass transport. In: *Topics in applied physics: Turbulence*, P. BRADSHAW, editor, Springer-Verlag, Berlin, pp. 231–287.

LAUNDER B. E. (1989) Second-moment closure; present . . . and future? *International Journal of Heat and Fluid Flow*, **10**, 282–300.

PANTIN H. M. (1979) Interaction between velocity and effective density in turbidity flows: phase-plane analysis, with criteria for autosuspension. *Marine Geology*, **31**, 59–99.

PANTIN H. M. (1986) Triggering of autosuspension by a periodic forcing function. In: *Proceedings of the Third International Symposium on River Sedimentation*, S. Y. WANG, H. W. SHEN and L. Z. DING, editors, School of Engineering, The University of Mississippi, Mississippi, USA.

RIBBERINK J. S. and A. A. AL-SALEM (1992) *Time dependent sediment transport phenomena in oscillatory boundary layer flow under sheet flow conditions*. Data report H 840, **20** Part VI. Delft Hydraulics.

ROTTA J. C. (1951) Statstische Theorie nichthomogener Turbulenz. *Z. Phys.* **129**, 547–572.

SHENG Y. P. (1984) A turbulent transport model of coastal processes. *Proceedings of the nineteenth International Conference on Coastal Engineering*, pp. 2380–2396.

SHENG Y. P. and C. VILLARET (1989) Modeling the effect of suspended sediment stratification on bottom exchange processes. *Journal of Geophysical Research*, **94(C10)**, 14,429–14,444.

SLEATH J. F. A. (1987) Turbulent oscillatory flow over rough beds. *Journal of Fluid Mechanics*, **182**, 369–409.

SUMER B. M., B. L. JENSEN and J. FREDSØE (1987) Turbulence in oscillatory boundary layers. In: *Advances in turbulences*, G. COMTE-BELOT and J. MATHIEU, editors, Springer Verlag, Berlin, pp. 556–567.

TELIONIS D. T. (1981) *Unsteady viscous flows*, Springer-Verlag, Berlin, 408 pp.